Structural Engineering and Mechanics, *Vol. 51, No. 4 (2014) 601-625*
DOI: http://dx.doi.org/10.12989/sem.2014.51.4.601

Large displacement geometrically nonlinear finite element analysis of 3D Timoshenko fiber beam element

Zhengzhou Hu[a] and Minger Wu[*]

Department of Building Engineering, Tongji University, Shanghai 200092, P.R. China

(Received March 1, 2013, Revised May 18, 2014, Accepted May 27, 2014)

Abstract. Based on continuum mechanics and the principle of virtual displacements, incremental total Lagrangian formulation (T.L.) and incremental updated Lagrangian formulation (U.L.) were presented. Both T.L. and U.L. considered the large displacement stiffness matrix, which was modified to be symmetrical matrix. According to the incremental updated Lagrangian formulation, small strain, large displacement, finite rotation of three dimensional Timoshenko fiber beam element tangent stiffness matrix was developed. Considering large displacement and finite rotation, a new type of tangent stiffness matrix of the beam element was developed. According to the basic assumption of plane section, the displacement field of an arbitrary fiber was presented in terms of nodal displacement of centroid of cross-area. In addition, shear deformation effect was taken account. Furthermore, a nonlinear finite element method program has been developed and several examples were tested to demonstrate the accuracy and generality of the three dimensional beam element.

Keywords: 3D Timoshenko fiber beam element; large displacement matrix; finite rotation; total Lagrangian formulation and updated Lagrangian formulation; incremental nonlinear finite element method

1. Introduction

Framed structures demonstrate highly nonlinear characteristic under ultimate load or strong earthquake, due to complicated mechanic performance of the reinforced concrete material, the accurate demand of the structural analysis is particularly significant very much. Zeris (1988, 1991) and Spacone (1996a, b) proposed fiber-model beam-column element based on flexibility method and stiffness method respectively, and then successfully solved the materially nonlinear problem of reinforced concrete columns. Nie (2012) used fiber beam element to analyze steel-concrete composite structures, and further studied the intrinsic mechanisms and failure law of these members. Li *et al*. (2012) used fiber beam element to simulate spatial concrete structures under fire, and found the progressive collapse mechanism and failure law of the structures. Zubydan and Elsabbagh (2011) developed a fiber model based on the fiber beam element to evaluate the monotonic and cyclic behavior of concrete-filled steel tube (CFST) beam-columns with rectangular cross section, and the local buckling effect of the CFST was considered yet. Huu and

*Corresponding author, Professor , E-mail: wuminger@tongji.edu.cn
[a]Ph.D. Student, E-mail: huzhengzhou@126.com

Copyright © 2014 Techno-Press, Ltd.
http://www.techno-press.org/?journal=sem&subpage=8 ISSN: 1225-4568 (Print), 1598-6217 (Online)

Seung (2011a, b) had done an effective nonlinear inelastic dynamic analysis of steel frames and concrete-filled steel tubular frames under dynamic loadings which considers both geometric and material nonlinearities using fiber hinge beam element. Huu and Seung (2012) proposed fiber hinge beam element to predict ultimate load-carrying capacity and ultimate behavior of cable-stayed bridges considering both geometric and material nonlinearities, in which the geometric nonlinearity was developed using stability functions obtained from the exact stability solution of a beam subjected to the coupling of axial force and bending moments. According to Euler-Bernoulli theory, Tort and Hajjar (2010) deduced a beam finite element formulation through adopting a mixed finite element method, and analyzed rectangular concrete-filled steel tube (RCFT) beam-columns, considering geometrical and material nonlinear. Therefore, fiber beam element is one of the most effective and accurate elements to analyze the highly nonlinear analysis of framed structures, but in view of the pioneering work, there does not appear to have been any attempt to develop those results to a three dimensional Timoshenko fiber beam element with shear effect be taken into account, and it is my main purpose to fill this gap in the paper.

Though Eduardo *et al.*(1988) developed an incremental Total Lagrangian formulation for curved beam elements that included the effect of large rotation and the effect shear influence, Crivelli and Felippa (1993) used the core-congruential formulation (CCF) to derive the discrete equations and studied a three dimensional geometrically nonlinear ,two-node Timoshenko beam element based on the Total Lagrangian description, Zhang *et al.*(2011) presented the small strain beam element stiffness by combining Timoshenko beam theory with fiber model which was implemented into software MSC. Marc, and then analyzed the nonlinear response of a deep beam, at last grave a satisfactory results. While author based on continuum mechanics and the principle of virtual displacements, and then developed incremental total Lagrangian formulation (T.L.) and incremental updated Lagrangian formulation (U.L.) in this paper respectively, at last presented small strain, large displacement, finite rotation of three dimensional Timoshenko fiber beam element tangent stiffness matrix based on U.L., in which the shear deformation effect was considered. In the assumption of the plane cross section, the displacement field of an arbitrary fiber was presented in terms of nodal point displacement of centroid of cross-area.

In addition, a nonlinear finite element method program has been developed, and strong and high accuracy and generality were achieved compared to the results of the published references.

2. Incremental T.L. and U.L. formulations

Base on continuum mechanics and the principle of virtual displacement, incremental nonlinear finite element methods formulation was induced considering the effect of large displacement (Bathe 1982)

$$\begin{aligned} &\int_{{}^{t+\Delta t}V} {}^{t+\Delta t}\boldsymbol{\tau}_{ij}\delta^{t+\Delta t}\boldsymbol{e}_{ij}\,{}^{t+\Delta t}dv={}^{t+\Delta t}\boldsymbol{R} \\ &{}^{t+\Delta t}\boldsymbol{R}=\int_{{}^{t+\Delta t}A} {}^{t+\Delta t}\boldsymbol{t}\delta\boldsymbol{u}_k\,{}^{t+\Delta t}da+\int_{{}^{t+\Delta t}V} {}^{t+\Delta t}\rho\,{}^{t+\Delta t}\boldsymbol{f}_k\delta\boldsymbol{u}_k\,{}^{t+\Delta t}dv+\delta\boldsymbol{u}_k\,{}^{t+\Delta t}\boldsymbol{q} \end{aligned} \tag{1}$$

Where ${}^{t+\Delta t}\boldsymbol{R}$ was the total external virtual work expression under the surface forces, body forces, and nodal point forces in the time $t+\Delta t$, ${}^{t+\Delta t}\boldsymbol{\tau}_{ij}$ was the Cauchy stress vector in the time $t+\Delta t$, $\delta^{t+\Delta t}\boldsymbol{\tau}_{ij}$ was the variation of Almansi strain vector in the time $t+\Delta t$, ${}^{t+\Delta t}dv$ was per differential volume variable in the time $t+\Delta t$, ${}^{t+\Delta t}\boldsymbol{t}$ was per area load in the time $t+\Delta t$, ${}^{t+\Delta t}\boldsymbol{\rho}$ was the density per volume

in the time $t+\Delta t$, $\delta \boldsymbol{u}_k$ was variation of virtual displacement vector, ${}^{t+\Delta t}da$ was per differential area variable in the time $t+\Delta t$, ${}^{t+\Delta t}\boldsymbol{f}_k$ was per volume load vector in the time $t+\Delta t$, , ${}^{t+\Delta t}\boldsymbol{q}$ was nodal load vector in the time $t+\Delta t$. The U.L. and T.L. were derived from the continuum mechanics based Lagrangian incremental equilibrium equations referring to the initial and time t configuration respectively.

2.1 Incremental T.L. mechanics formulation referring to initial configuration

Eq. (1) was defined in the initial configuration, we gave

$$\begin{aligned} &\int_{{}^0V} {}^{t+\Delta t}_{\ \ 0}\boldsymbol{S}\delta {}^{t+\Delta t}_{\ \ 0}\boldsymbol{E}\,{}^0dv = {}^{t+\Delta t}\boldsymbol{R} \\ &{}^{t+\Delta t}\boldsymbol{R} = \int_{{}^0A} {}^{t+\Delta t}_{\ \ 0}\boldsymbol{t}\delta \boldsymbol{u}_k\,{}^0da + \int_{{}^0V} {}^{t+\Delta t}_{\ \ 0}\rho\, {}^{t+\Delta t}_{\ \ 0}\boldsymbol{f}\,{}^0dv + \delta \boldsymbol{u}_k\, {}^{t+\Delta t}_{\ \ 0}\boldsymbol{q} \end{aligned} \tag{2}$$

Where ${}^{t+\Delta t}_{\ \ 0}\boldsymbol{S}$ was 2nd Piola-Kirchhoff stress vector in the time $t+\Delta t$ referring to the initial configuration time 0, $\delta {}^{t+\Delta t}_{\ \ 0}\boldsymbol{E}$ was variation of Green strain vector in the time $t+\Delta t$ referring to the initial configuration referring to the papers (Bathe and Wilson 1974, Bathe *et al*. 1975, Bathe and Bolourch 1979), ${}^0da$ was per differential area variable in the time $t+\Delta t$ referring to time 0,${}^0dv$ was per differential volume variable in the time 0

$$\begin{aligned} &\int_{{}^0V} [(\delta\{\Delta \boldsymbol{E}^L_{ij}\}^T + \delta\{\Delta \boldsymbol{E}^N_{ij}\}^T)\,{}^t_0\{\boldsymbol{S}\} + (\delta\{\Delta \boldsymbol{E}^L_{ij}\}^T + \delta\{\Delta \boldsymbol{E}^N_{ij}\}^T)\boldsymbol{D}_T([\boldsymbol{B}_L] + \frac{1}{2}[\boldsymbol{B}]_N)\{\Delta \boldsymbol{u}_e\}]^0dv \\ &= \left(\delta\{\Delta \boldsymbol{u}_e\}\right)^T {}^{t+\Delta t}_{\ \ 0}\{\boldsymbol{q}\} + \int_{{}^0V} \delta\{\Delta \boldsymbol{u}_e\}^T\, {}^{t+\Delta t}_{\ \ 0}\rho\, {}^{t+\Delta t}_{\ \ 0}\{\boldsymbol{f}\}^0dv + \int_{{}^0A} \delta(\Delta \boldsymbol{u}_e)^T\, {}^{t+\Delta t}_{\ \ 0}\{\boldsymbol{t}\}^0da \end{aligned} \tag{3}$$

Where $\Delta \boldsymbol{E}^L_{ij}$ was linearly incremental strains, $\Delta \boldsymbol{E}^N_{ij}$ was nonlinearly incremental Green strain, $\{\boldsymbol{S}\}$ was 2nd Piola-Kirchhoff stress vector, $\delta\{\Delta \boldsymbol{u}_e\}$ is variation of displacement vector of element, ${}^{t+\Delta t}_{\ \ 0}\{\boldsymbol{q}\}$ was nodal load in the time $t+\Delta t$ referring to time 0, ${}^{t+\Delta t}_{\ \ 0}\rho$ was the density per volume in the time $t+\Delta t$ referring to time 0, ${}^{t+\Delta t}_{\ \ 0}\{\boldsymbol{f}_k\}$ was per volume load vector in the time $t+\Delta t$ referring to time 0. Considering $\delta\{\Delta \boldsymbol{u}_e\}$ arbitrary, Eq. (3) was simplified as followings, variable $t+\Delta t$ in the top left corner and variable 0 in the lower left corner were neglected in the initial configuration

$$\begin{aligned} &([\boldsymbol{k}_L] + [\boldsymbol{k}_\sigma] + [\boldsymbol{k}_U])\{\Delta \boldsymbol{u}_e\} \\ &= [\boldsymbol{N}]^T\, {}^{t+\Delta t}_{\ \ 0}\{\boldsymbol{q}\} + \int_{{}^0V} [\boldsymbol{N}]^T\, {}^{t+\Delta t}_{\ \ 0}\rho\, {}^{t+\Delta t}_{\ \ 0}\{\boldsymbol{f}\}^0dv + \int_{{}^0A} [\boldsymbol{N}]^T\, {}^{t+\Delta t}_{\ \ 0}\{\boldsymbol{t}\}^0da - \int_{{}^0V} [\boldsymbol{B}_L]^T\, {}^t_0\boldsymbol{S}\,{}^0dv \end{aligned} \tag{4}$$

Eq. (4) $[\boldsymbol{k}_L], [\boldsymbol{k}_\sigma], [\boldsymbol{k}_U]$

$$[\boldsymbol{k}_L] = \int_{{}^0V} [\boldsymbol{B}_L]^T [\boldsymbol{D}_T][\boldsymbol{B}_L]^0dv \tag{5}$$

$$[\boldsymbol{k}_\sigma] = \int_{{}^0V} [\boldsymbol{G}]^T\, {}^t_0[\boldsymbol{M}][\boldsymbol{G}]^0dv \tag{6}$$

$$[\boldsymbol{k}_U]=\int_{{}^0V}(\frac{1}{2}[\boldsymbol{B}_L]^T[\boldsymbol{D}_T][\boldsymbol{B}_N]+[\boldsymbol{B}_N]^T[\boldsymbol{D}_T][\boldsymbol{B}_L]+\frac{1}{2}[\boldsymbol{B}_N]^T[\boldsymbol{D}_T][\boldsymbol{B}_N])^0dv \tag{7}$$

Where, $[\boldsymbol{D}_T]$ was the tangent constitutive matrix relating small strain increments to the corresponding stress increments. $[\boldsymbol{B}_L]$ was linear transform matrix relating to strains to displacement. $[\boldsymbol{B}_N]$ was nonlinear transform matrix relating to strains to displacement, $[\boldsymbol{G}]$ is transform matrix of incremental displacement vector, $[\boldsymbol{M}]$ is stress incremental matrix. $[\boldsymbol{N}]$ was the interpolation functions corresponding to the local axes relating to displacement function to the nodal point displacement. $[\boldsymbol{k}_L]$ was linear strain incremental stiffness matrices. $[\boldsymbol{k}_\sigma]$ was nonlinear strain (geometric or initial stress) incremental stiffness matrices. $[\boldsymbol{k}_U]$ was large displacement matrices caused by incremental displacement of nodal point.

When Bathe (1982) induced the T.L. formulation, the $[\boldsymbol{k}_U]$ was neglected, whereas Hibbitt (1970) induced the incremental equilibrium equation, the $[\boldsymbol{k}_U]$ was established. Due to the $[\boldsymbol{k}_U]$ matrix was asymmetric, the matrix was modified to be symmetric in this paper as follows

$$\begin{aligned}[\boldsymbol{k}_U]&=\int_{{}^0V}(\frac{1}{2}[\boldsymbol{B}_L]^T[\boldsymbol{D}_T][\boldsymbol{B}_N]+[\boldsymbol{B}_N]^T[\boldsymbol{D}_T][\boldsymbol{B}_L]+\frac{1}{2}[\boldsymbol{B}_N]^T[\boldsymbol{D}_T][\boldsymbol{B}_N])^0dv\\&\approx\int_{{}^0V}(\frac{1}{2}[\boldsymbol{B}_L]^T[\boldsymbol{D}_T][\boldsymbol{B}_N]+\frac{1}{2}[\boldsymbol{B}_N]^T[\boldsymbol{D}_T][\boldsymbol{B}_L]+\frac{1}{2}[\boldsymbol{B}_N]^T[\boldsymbol{D}_T][\boldsymbol{B}_N])^0dv\\&=\frac{1}{2}\int_{{}^0V}([\boldsymbol{B}_L]^T[\boldsymbol{D}_T][\boldsymbol{B}_N]+[\boldsymbol{B}_N]^T[\boldsymbol{D}_T][\boldsymbol{B}_L]+[\boldsymbol{B}_N]^T[\boldsymbol{D}_T][\boldsymbol{B}_N])^0dv\end{aligned} \tag{8}$$

2.2 Incremental U.L. mechanics formulation referring to current time configuration

According to relationship of conjugated energy, Eq. (1) was redefined in the time t configuration

$$\begin{aligned}&\int_{{}^{t+\Delta t}V}{}^{t+\Delta t}\boldsymbol{\tau}\delta^{t+\Delta t}\boldsymbol{e}dv=\int_{{}^{t+\Delta t}V}{}^{t+\Delta t}_{t}\boldsymbol{S}\delta^{t+\Delta t}_{t}\boldsymbol{E}dv\\&=\left(\delta\{\Delta\boldsymbol{u}_e\}\right)^T{}^{t+\Delta t}_{t}\{\boldsymbol{q}\}+\int_{{}^tV}\delta\{\Delta\boldsymbol{u}_e\}^T{}^{t+\Delta t}_{t}\rho^{t+\Delta t}_{t}\{\boldsymbol{f}\}^tdv+\int_{{}^tA}\delta(\Delta\boldsymbol{u}_e)^T{}^{t+\Delta t}_{t}\{\boldsymbol{t}\}^tda\end{aligned} \tag{9}$$

In accordance with the reference (Bathe 1982)

$$\begin{aligned}&([\boldsymbol{k}_L]+[\boldsymbol{k}_\sigma]+[\boldsymbol{k}_U])\{\Delta\boldsymbol{u}_e\}\\&=[\boldsymbol{N}]^T{}^{t+\Delta t}_{t}\{\boldsymbol{q}\}+\int_{{}^tV}[\boldsymbol{N}]^T{}^{t+\Delta t}_{t}\rho^{t+\Delta t}_{t}\{\boldsymbol{f}\}^tdv+\int_{{}^tA}[\boldsymbol{N}]^T{}^{t+\Delta t}_{t}\{\boldsymbol{t}\}^tda-\int_{{}^tV}[\boldsymbol{B}_L]^T{}^t_t\boldsymbol{S}^tdv\end{aligned} \tag{10}$$

Equations as follows were induced referring to the time t configuration, and then variable $t+\Delta t$ in the top left corner and variable 0 in the lower left corner were neglected in the time t configuration, the matrices of $[\boldsymbol{k}_L]$, $[\boldsymbol{k}_\sigma]$ and $[\boldsymbol{k}_U]$ were defined as follows

$$[\boldsymbol{k}_L]=\int_{{}^tV}[\boldsymbol{B}_L]^T[\boldsymbol{D}_T][\boldsymbol{B}_L]^tdv \tag{11}$$

$$[\boldsymbol{k}_\sigma]=\int_{{}^tV}[\boldsymbol{G}]^T[\boldsymbol{M}][\boldsymbol{G}]^tdv \tag{12}$$

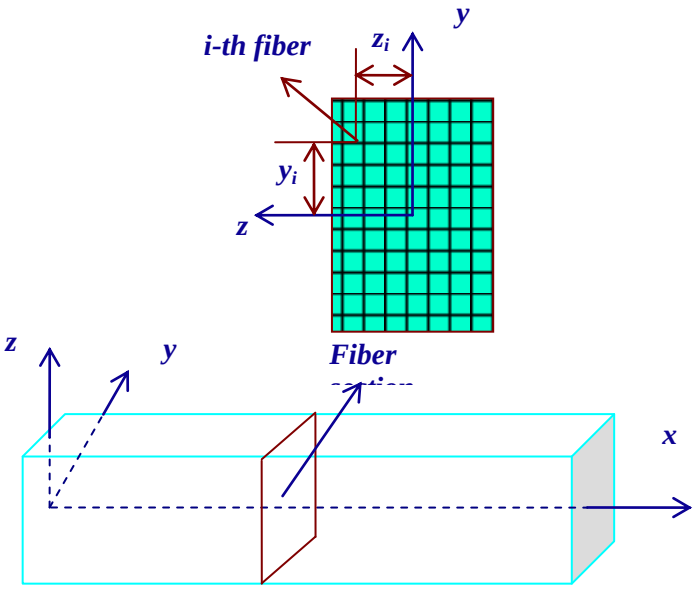

Fig. 1 Three dimensional Timoshenko fiber beam element

$$[\boldsymbol{k}_U]=\int_{{}^tV}\left(\frac{1}{2}[\boldsymbol{B}_L]^T[\boldsymbol{D}_T][\boldsymbol{B}_N]+[\boldsymbol{B}_N]^T[\boldsymbol{D}_T][\boldsymbol{B}_L]+\frac{1}{2}[\boldsymbol{B}_N]^T[\boldsymbol{D}_T][\boldsymbol{B}_N]\right)^t dv \tag{13}$$

$[\boldsymbol{k}_U]$ matrix of Eq. (13) was still asymmetric, the author simplified the matrix

$$\begin{aligned}[\boldsymbol{k}_U]&=\int_{{}^tV}\left(\frac{1}{2}[\boldsymbol{B}_L]^T[\boldsymbol{D}_T][\boldsymbol{B}_N]+[\boldsymbol{B}_N]^T[\boldsymbol{D}_T][\boldsymbol{B}_L]+\frac{1}{2}[\boldsymbol{B}_N]^T[\boldsymbol{D}_T][\boldsymbol{B}_N]\right)^t dv\\ &\approx\int_{{}^tV}\left(\frac{1}{2}[\boldsymbol{B}_L]^T[\boldsymbol{D}_T][\boldsymbol{B}_N]+\frac{1}{2}[\boldsymbol{B}_N]^T[\boldsymbol{D}_T][\boldsymbol{B}_L]+\frac{1}{2}[\boldsymbol{B}_N]^T[\boldsymbol{D}_T][\boldsymbol{B}_N]\right)^t dv\\ &=\frac{1}{2}\int_{{}^tV}\left([\boldsymbol{B}_L]^T[\boldsymbol{D}_T][\boldsymbol{B}_N]+[\boldsymbol{B}_N]^T[\boldsymbol{D}_T][\boldsymbol{B}_L]+[\boldsymbol{B}_N]^T[\boldsymbol{D}_T][\boldsymbol{B}_N]\right)^t dv\end{aligned} \tag{14}$$

And then $[\boldsymbol{k}_U]$ was made to be symmetric, causing the total of tangent stiffness symmetric, whereas Bathe (1982, 1975, 1979) induced the incremental U.L. formulation, the matrix was neglected, which was reserved in this paper considering effect of high order displacement.

Through above mentioned theory, the U.L. and T.L. were induced, furthermore the large displacement matrix was modified, which made the storage of tangent stiffness in memory favorable in order to have the advantage of solving the equilibrium equations. In essence, the incremental T.L. formulation and incremental U.L. formulation were the same, they were described based on Lagrangematerial, the former was defined in the initial configuration, while the latter was defined in the time *t* configuration.

3. Derivation of 3D Timoshenko fiber beam element stiffness

3.1 Derivation linear strain incremental stiffness matrices

Displacement field of arbitrary point in the element was defined in the local coordinate system as follows (Bazoune *et al*. 2003), see Fig. 1

$$\begin{Bmatrix} u(x,y,z) \\ v(x,y,z) \\ w(x,y,z) \end{Bmatrix} = \begin{bmatrix} 1-\frac{x}{L} & 0 & 0 & 0 & 0 & 0 & \frac{x}{L} & 0 & 0 & 0 & 0 & 0 \\ 0 & N_{2,2} & 0 & 0 & 0 & N_{2,6} & 0 & N_{2,8} & 0 & 0 & 0 & N_{2,12} \\ 0 & 0 & N_{3,3} & 0 & N_{3,5} & 0 & 0 & 0 & N_{3,9} & 0 & N_{3,11} & 0 \\ 0 & 0 & 0 & \frac{L-x}{L} & 0 & 0 & 0 & 0 & 0 & \frac{x}{L} & 0 & 0 \\ 0 & 0 & N_{5,3} & 0 & N_{5,5} & 0 & 0 & 0 & N_{5,9} & 0 & N_{5,11} & 0 \\ 0 & N_{6,2} & 0 & 0 & 0 & N_{6,6} & 0 & N_{6,8} & 0 & 0 & 0 & N_{6,12} \end{bmatrix} \{\boldsymbol{u}\} \tag{15}$$

Where, the elements of right side of Eq. (15) can be particularly expressed in following

$$N_{2,2} = \frac{1}{\Phi_z L^3}\left(2x^3 - 3Lx^2 - \Phi_z xL^2 + xL^2 + \Phi_z L^3\right), N_{2,6} = \frac{1}{2\Phi_z L^2}\left(2x^3 - 3Lx^2 - \Phi_z Lx^2 + xL^2 + \Phi_z xL^2\right)$$

$$N_{2,8} = \frac{1}{\Phi_z L^3}\left(\Phi_z xL^2 - xL^2 + 3x^2 L - 2x^3\right), N_{2,12} = \frac{1}{2\Phi_z L^2}\left(2x^3 - 3Lx^2 + \Phi_z Lx^2 + xL^2 - \Phi_z xL^2\right)$$

$$N_{3,3} = \frac{1}{\Phi_y L^3}\left(2x^3 - 3Lx^2 - \Phi_y xL^2 + xL^2 + \Phi_y L^3\right), N_{3,5} = \frac{1}{2\Phi_y L^2}\left(-\Phi_y xL^2 - xL^2 + \Phi_y Lx^2 + 3Lx^2 - 2x^3\right)$$

$$N_{3,9} = \frac{1}{\Phi_y L^3}\left(\Phi_y xL^2 - xL^2 + 3Lx^2 - 2x^3\right), N_{3,11} = \frac{1}{2\Phi_y L^2}\left(\Phi_y xL^2 - xL^2 - \Phi_y Lx^2 + 3Lx^2 - 2x^3\right)$$

$$N_{5,3} = \frac{1}{\Phi_y L^3}\left(6xL - 6x^2\right), N_{5,5} = \frac{1}{\Phi_y L^2}\left(3x^2 - \Phi_y xL - 3xL + \Phi_y L^2\right), N_{5,9} = \frac{1}{\Phi_y L^3}\left(6x^2 - 6xL\right)$$

$$N_{5,11} = \frac{1}{\Phi_y L^2}\left(3x^2 - 3xL + \Phi_y xL\right), N_{6,2} = \frac{1}{\Phi_z L^3}\left(6x^2 - 6xL\right), N_{6,6} = \frac{1}{\Phi_z L^2}\left(3x^2 - \Phi_z xL - 3xL + \Phi_z L^2\right)$$

$$N_{6,8} = \frac{1}{\Phi_z L^3}\left(6xL - 6x^2\right), N_{6,12} = \frac{1}{\Phi_z L^2}\left(3x^2 - 3xL + \Phi_z xL\right)$$

And where

$$\Phi_y = 1 + \frac{12EI_y}{\kappa_z GAL^2} \ , \ \Phi_z = 1 + \frac{12EI_z}{\kappa_y GAL^2}$$

Where L was length of the beam element, x was length along the local coordinate x axis from the node one, κ_y was shear correction factor that accounts for the non-uniform distribution of the shear stress over the cross-section A, I_y was the second moment of area about y-axis, I_z was the second moment of area about z-axis, v was poisson's ratio, E was modulus of elasticity, G was shear modulus.

Strain of arbitrary fiber in cross-section was defined as follows

$$\{\varepsilon\} = \begin{Bmatrix} \varepsilon_{11} \\ \varepsilon_{12} \\ \varepsilon_{13} \\ \varepsilon_{23} \end{Bmatrix} \tag{16}$$

Where, ε_{11} was axial strain, ε_{12} was shear strain xy, ε_{13} was shear strain xz, ε_{23} was shear strain yz

corresponding to axial stress σ_{11}, shear stress *xy* τ_{xy}, shear stress *xz* τ_{xz}, shear stress *yz* τ_{yz}, they were defined as follows, where E_i is elastic modulus of *i* fiber, G_i is shear elastic modulus of *i* fiber.

$$\{\boldsymbol{\sigma}\}=\begin{Bmatrix}\sigma_{11}\\ \tau_{xy}\\ \tau_{xz}\\ \tau_{yz}\end{Bmatrix}=\boldsymbol{D\varepsilon}=\begin{bmatrix}E_i & 0 & 0 & 0\\ 0 & G_i & 0 & 0\\ 0 & 0 & G_i & 0\\ 0 & 0 & 0 & G_i\end{bmatrix}\begin{Bmatrix}\varepsilon_{11}\\ \varepsilon_{12}\\ \varepsilon_{13}\\ \varepsilon_{23}\end{Bmatrix} \tag{17}$$

Strain of centroid of cross-section was ($\varepsilon_0\ \varepsilon_{12}\ \varepsilon_{13}\ \varepsilon_{23}$), we gave

$$\varepsilon_0=u'=\frac{du}{dx} \tag{18}$$

Axial strain of arbitrary fiber in the cross-section was defined as follows

$$\varepsilon_{11}=\varepsilon_0-yv''+zw'' \tag{19}$$

Where, *u*, *v*, *w* are displacement function along *x*, *y*, *z* direction of local coordinate respectively, see Fig. 1.

Strain of arbitrary fiber of cross-area was defined as follows

$$\{\boldsymbol{\varepsilon}_L\}=\begin{Bmatrix}\varepsilon_{11}\\ \varepsilon_{12}\\ \varepsilon_{23}\\ \varepsilon_{13}\end{Bmatrix}=\begin{Bmatrix}\dfrac{\partial(u-y\theta_z+z\theta_y)}{\partial x}\\ \dfrac{\partial(u-y\theta_z+z\theta_y)}{\partial y}+\dfrac{\partial(v-z\theta_x)}{\partial x}\\ \dfrac{\partial(v-z\theta_x)}{\partial z}+\dfrac{\partial(w+y\theta_x)}{\partial y}\\ \dfrac{\partial(u-y\theta_z+z\theta_y)}{\partial z}+\dfrac{\partial(w+y\theta_x)}{\partial x}\end{Bmatrix}=\begin{bmatrix}1 & 0 & 0 & 0 & z & -y\\ 0 & 1 & 0 & -z & 0 & 0\\ 0 & 0 & 0 & 0 & 0 & 0\\ 0 & 0 & 1 & y & 0 & 0\end{bmatrix}\begin{Bmatrix}u'\\ v'-\theta_z\\ w'+\theta_y\\ v''\\ w''\\ \theta_x'\end{Bmatrix}=[\boldsymbol{b}]\{\boldsymbol{s}\} \tag{20}$$

Where θ_x, θ_y, θ_z are rotational angle variable along *x*, *y*, *z* direction of local coordinate respectively, see Fig. 1. Stress of arbitrary fiber in cross-section was defined as follows

$$\{\boldsymbol{\sigma}\}=\begin{Bmatrix}\sigma_{11}\\ \tau_{xy}\\ \tau_{xz}\\ \tau_{yz}\end{Bmatrix}=\boldsymbol{D\varepsilon}=\begin{bmatrix}E_i & 0 & 0 & 0\\ 0 & G_i & 0 & 0\\ 0 & 0 & G_i & 0\\ 0 & 0 & 0 & G_i\end{bmatrix}\begin{Bmatrix}\varepsilon_{11}\\ \varepsilon_{12}\\ \varepsilon_{13}\\ \varepsilon_{23}\end{Bmatrix}=[\boldsymbol{D}][\boldsymbol{b}]\{\boldsymbol{s}\} \tag{21}$$

The $\{\boldsymbol{s}\}$ of above equation was also redefined as follows

$$\{\boldsymbol{s}\}=\begin{Bmatrix}\dfrac{du}{dx}\\ \dfrac{dv}{dx}-\theta_z\\ \dfrac{dw}{dx}-\theta_y\\ \dfrac{d^2v}{dx^2}\\ \dfrac{d^2w}{dx^2}\\ \dfrac{d\theta_x}{dx}\end{Bmatrix}=\begin{Bmatrix}\dfrac{du}{dx}\\ \dfrac{dv}{dx}-\theta_z\\ \dfrac{dw}{dx}-\theta_y\\ \dfrac{d\theta_z}{dx}\\ -\dfrac{d\theta_y}{dx}\\ \dfrac{d\theta_x}{dx}\end{Bmatrix} \tag{22}$$

On the basis of variational theorem of energy function of the cross-section, we gave

$$\begin{aligned}\Pi_e &= \int \frac{1}{2}\{\boldsymbol{\varepsilon}\}^T\{\boldsymbol{\sigma}\}dA - \{\boldsymbol{s}\}^T\{\boldsymbol{f}_s\} \\ &= \frac{1}{2}\{\boldsymbol{s}\}^T\int[\boldsymbol{b}]^T[\boldsymbol{D}][\boldsymbol{b}]dA\{\boldsymbol{s}\} - \{\boldsymbol{s}\}^T\{\boldsymbol{f}_s\}\end{aligned} \tag{23}$$

Based on the potential energy, the $\{\boldsymbol{s}\}$ was derived by calculus of variation

$$\delta\Pi_e = \frac{\delta\Pi_e}{\delta\{\boldsymbol{s}\}}\delta\{\boldsymbol{s}\} = 0 \tag{24}$$

Due to $\delta\{\boldsymbol{s}\}$ arbitrary

$$\frac{\delta\Pi_e}{\delta\{\boldsymbol{s}\}} = \int[\boldsymbol{b}]^T[\boldsymbol{D}][\boldsymbol{b}]dA\{\boldsymbol{s}\} - \{\boldsymbol{f}_s\} = 0 \tag{25}$$

The Eq. (26) was simplified as follows

$$[\boldsymbol{K}_s]\{\boldsymbol{s}\} = \{\boldsymbol{f}\} \tag{26}$$

Where $[\boldsymbol{K}_s]$ was tangent stiffness matrix of cross-section, and then expressed as follows

$$[\boldsymbol{k}_s] = \int[\boldsymbol{b}]^T[\boldsymbol{D}][\boldsymbol{b}]dA$$

$$= \begin{bmatrix} \sum_{i=1}^{n}E_iA_i & 0 & 0 & 0 & \sum_{i=1}^{n}E_iA_iz_i & -\sum_{i=1}^{n}E_iA_iy_i \\ 0 & \sum_{i=1}^{n}G_iA_i & 0 & -\sum_{i=1}^{n}G_iA_iz_i & 0 & 0 \\ 0 & 0 & \sum_{i=1}^{n}G_iA_i & \sum_{i=1}^{n}G_iA_iy_i & 0 & 0 \\ 0 & -\sum_{i=1}^{n}G_iA_iz_i & \sum_{i=1}^{n}G_iA_iy_i & \sum_{i=1}^{n}G_iA_i(y_i^2+z_i^2) & 0 & 0 \\ \sum_{i=1}^{n}E_iA_iz_i & 0 & 0 & 0 & \sum_{i=1}^{n}E_iA_iz_i^2 & -\sum_{i=1}^{n}E_iA_iy_iz_i \\ -\sum_{i=1}^{n}E_iA_iy_i & 0 & 0 & 0 & -\sum_{i=1}^{n}E_iA_iy_iz_i & \sum_{i=1}^{n}E_iA_iy_i^2 \end{bmatrix}_{6\times6}$$

Where A_i was area of area of i fiber, y_i, z_i were coordinate of i fiber in local coordinate, please see Fig. 1. The force vector $\{\boldsymbol{f}_s\}$ of cross-section of beam element was defined as follows

$$\{\boldsymbol{f}_s\} = \left\{\sum_{i=1}^{n}\sigma_{11}A_i \quad \sum_{i=1}^{n}\sigma_{12}A_i \quad \sum_{i=1}^{n}\sigma_{13}A_i \quad \sum_{i=1}^{n}\left(-z\cdot\sigma_{12}A_i + y\cdot\sigma_{13}A_i\right) \quad \sum_{i=1}^{n}z\cdot\sigma_{11}A_i \quad \sum_{i=1}^{n}-y\cdot\sigma_{11}A_i\right\}^T \tag{27}$$

By making use of the principle of virtual work and variational theorem, and then according to Eq. (11), we gave linear strain stiffness matrix as follows

$$[\boldsymbol{k}_L]^e = \int_L[\boldsymbol{B}_L(x)]^T[\boldsymbol{k}_s][\boldsymbol{B}_L(x)]dx \tag{28}$$

Where $[\boldsymbol{B}_L]$

$$[\boldsymbol{B}_L]=\begin{bmatrix} -\frac{1}{L} & 0 & 0 & 0 & 0 & 0 & \frac{1}{L} & 0 & 0 & 0 & 0 & 0 \\ 0 & B_{2,2} & 0 & 0 & 0 & B_{2,6} & 0 & B_{2,8} & 0 & 0 & 0 & B_{2,12} \\ 0 & 0 & B_{3,3} & 0 & B_{3,5} & 0 & 0 & 0 & B_{3,9} & 0 & B_{3,11} & 0 \\ 0 & 0 & 0 & -\frac{1}{L} & 0 & 0 & 0 & 0 & 0 & \frac{1}{L} & 0 & 0 \\ 0 & 0 & B_{5,3} & 0 & B_{5,5} & 0 & 0 & 0 & B_{5,9} & 0 & B_{5,11} & 0 \\ 0 & B_{6,2} & 0 & 0 & 0 & B_{6,6} & 0 & B_{6,8} & 0 & 0 & 0 & B_{6,12} \end{bmatrix}$$

And, the components of $[\boldsymbol{B}_L]$ were expressed in the following form,

$$B_{22}=-\frac{1}{L}+\frac{1}{\Phi_z L}, B_{2,6}=-\frac{1}{2}+\frac{1}{2\Phi_z}, B_{2,8}=-\frac{1}{\Phi_z L}+\frac{1}{L}, B_{2,12}=-\frac{1}{2}+\frac{1}{2\Phi_z}$$

$$B_{3,3}=\frac{1}{L}-\frac{1}{\Phi_y L}, B_{3,5}=-\frac{1}{2}+\frac{1}{2\Phi_y}, B_{3,9}=\frac{1}{\Phi_y L}-\frac{1}{L}, B_{3,11}=-\frac{1}{2}+\frac{1}{2\Phi_y}$$

$$B_{5,3}=-\frac{12x}{\Phi_y L^3}+\frac{6}{\Phi_y L^2}, B_{5,5}=\frac{6x}{\Phi_y L^2}-\frac{1}{L}-\frac{3}{\Phi_y L}, B_{5,9}=\frac{12x}{\Phi_y L^3}-\frac{6}{\Phi_y L^2}, B_{5,11}=\frac{6x}{\Phi_y L^2}+\frac{1}{L}-\frac{3}{\Phi_y L}$$

$$B_{6,2}=\frac{12x}{\Phi_z L^3}-\frac{6}{\Phi_z L^2}, B_{6,6}=\frac{6x}{\Phi_z L^2}-\frac{1}{L}-\frac{3}{\Phi_z L}, B_{6,8}=-\frac{12x}{\Phi_z L^3}+\frac{6}{\Phi_z L^2}, B_{6,12}=\frac{6x}{\Phi_z L^2}+\frac{1}{L}-\frac{3}{\Phi_z L}$$

3.2 Derivation geometric stiffness matrix

Nonlinear Green strain $\boldsymbol{\varepsilon}_{NL}$ was defined as follows

$$\boldsymbol{\varepsilon}_{NL}=\begin{Bmatrix} \frac{1}{2}\left(\frac{\partial(u-y\theta_z+z\theta_y)}{\partial x}\right)^2+\frac{1}{2}\left(\frac{\partial(v-z\theta_x)}{\partial x}\right)^2+\frac{1}{2}\left(\frac{\partial(w+y\theta_x)}{\partial x}\right)^2 \\ \left(\frac{\partial(u-y\theta_z+z\theta_y)}{\partial x}\right)\cdot\left(\frac{\partial(u-y\theta_z+z\theta_y)}{\partial y}\right)+\left(\frac{\partial(v-z\theta_x)}{\partial x}\right)\left(\frac{\partial(v-z\theta_x)}{\partial y}\right)+\left(\frac{\partial(w+y\theta_x)}{\partial x}\right)\left(\frac{\partial(w+y\theta_x)}{\partial y}\right) \\ \left(\frac{\partial(u-y\theta_z+z\theta_y)}{\partial y}\right)\cdot\left(\frac{\partial(u-y\theta_z+z\theta_y)}{\partial z}\right)+\left(\frac{\partial(v-z\theta_x)}{\partial y}\right)\left(\frac{\partial(v-z\theta_x)}{\partial z}\right)+\left(\frac{\partial(w+y\theta_x)}{\partial y}\right)\left(\frac{\partial(w+y\theta_x)}{\partial z}\right) \\ \left(\frac{\partial(u-y\theta_z+z\theta_y)}{\partial x}\right)\cdot\left(\frac{\partial(u-y\theta_z+z\theta_y)}{\partial z}\right)+\left(\frac{\partial(v-z\theta_x)}{\partial x}\right)\left(\frac{\partial(v-z\theta_x)}{\partial z}\right)+\left(\frac{\partial(w+y\theta_x)}{\partial x}\right)\left(\frac{\partial(w+y\theta_x)}{\partial z}\right) \end{Bmatrix} \tag{29}$$

$$=\frac{1}{2}[\boldsymbol{A}][\boldsymbol{\theta}]$$

Where

$$[\boldsymbol{A}]=\begin{bmatrix} u'-y\theta_z'+z\theta_y' & v'-z\theta_x' & w'+y\theta_x' & 0 & 0 & 0 \\ -\theta_z & 0 & \theta_x & w'+y\theta_x' & 0 & -u'+y\theta_z'-z\theta_y' \\ 0 & 0 & 0 & 0 & -\theta_z & -\theta_y \\ \theta_y & -\theta_x & 0 & -v'+z\theta_x' & u'-y\theta_z'+z\theta_y' & 0 \end{bmatrix} \tag{30}$$

$$[\boldsymbol{\theta}]=\{u'-y\theta_z'+z\theta_y' \quad v'-z\theta_x' \quad w'+y\theta' \quad \theta_x \quad \theta_y \quad \theta_z\}^T$$

Where, θ_x was torsional displacement about x axis in the local coordinate system, θ_y was rotational displacement about y axis in the local coordinate system, θ_z was rotational displacement

about z axis in the local coordinate system. $[\boldsymbol{\theta}]$ can be expressed in the following form

$$[\boldsymbol{\theta}]=\begin{bmatrix}1&0&0&0&0&0&0&z&-y\\0&1&0&0&0&0&-z&0&0\\0&0&1&0&0&0&y&0&0\\0&0&0&1&0&0&0&0&0\\0&0&0&0&1&0&0&0&0\\0&0&0&0&0&1&0&0&0\end{bmatrix}[\boldsymbol{G}]\{\boldsymbol{u}\}_e$$
$$=[\overline{\boldsymbol{G}}]\{u\}_e$$

Where, $[\overline{\boldsymbol{G}}]$ was redefined in the following style of matrix

$$[\overline{\boldsymbol{G}}]=\begin{bmatrix}1&0&0&0&0&0&0&z&-y\\0&1&0&0&0&0&-z&0&0\\0&0&1&0&0&0&y&0&0\\0&0&0&1&0&0&0&0&0\\0&0&0&0&1&0&0&0&0\\0&0&0&0&0&1&0&0&0\end{bmatrix}[\boldsymbol{G}] \tag{31}$$
$$=[\boldsymbol{a}][\boldsymbol{G}]$$

Nonlinear Incremental strain $\boldsymbol{E}_{NL}$ can be defined as

$$\boldsymbol{E}_{NL}=[\boldsymbol{B}_{NL}]\{\boldsymbol{u}\}_e=[\boldsymbol{A}][\boldsymbol{G}]\{\boldsymbol{u}\}_e \tag{32}$$

Substituting incremental strain matrix $d\boldsymbol{B}$ into Eq. (33), we obtained

$$\left(d\boldsymbol{B}^T\right)\boldsymbol{S}=\left(d\boldsymbol{B}_{NL}{}^T\right)\boldsymbol{S}=[\overline{\boldsymbol{G}}]^T d\boldsymbol{A}^T\boldsymbol{S} \tag{33}$$

Where $d\boldsymbol{A}^T\boldsymbol{S}$ can be expressed as

$$d\boldsymbol{A}^T\boldsymbol{S}=\begin{bmatrix}u'-y\theta_z'+z\theta_y' & v'-z\theta_x' & w'+y\theta_x' & 0 & 0 & 0\\ -\theta_z & 0 & \theta_x & w'+y\theta_x' & 0 & -u'+y\theta_z'-z\theta_y'\\ 0 & 0 & 0 & 0 & -\theta_z & -\theta_y\\ \theta_y & -\theta_x & 0 & -v'+z\theta_x' & u'-y\theta_z'+z\theta_y' & 0\end{bmatrix}^T\{\boldsymbol{S}\}$$
$$=\begin{bmatrix}\sigma_{11}&0&0&0&\sigma_{31}&-\sigma_{12}\\0&\sigma_{11}&0&-\sigma_{31}&0&0\\0&0&\sigma_{11}&\sigma_{12}&0&0\\0&-\sigma_{31}&\sigma_{12}&0&0&0\\\sigma_{31}&0&0&0&0&-\sigma_{23}\\-\sigma_{12}&0&0&0&-\sigma_{23}&0\end{bmatrix}\{\boldsymbol{\theta}\}$$

Eq. (33) was also expressed as following

$$\begin{aligned}\left(d\boldsymbol{B}^T\right)\boldsymbol{S} &= \left(d\boldsymbol{B}_{NL}{}^T\right)\boldsymbol{S} = \left[\overline{\boldsymbol{G}}\right]^T\left[\overline{\boldsymbol{M}}\right]\left[\overline{\boldsymbol{G}}\right]d\left\{\boldsymbol{u}\right\}_e \\ &= \left[\boldsymbol{G}\right]^T\left[\boldsymbol{a}\right]^T\left[\overline{\boldsymbol{M}}\right]\left[\boldsymbol{a}\right]\left[\boldsymbol{G}\right]d\left\{\boldsymbol{u}\right\}_e \\ &= \left[\boldsymbol{G}\right]^T\left[\boldsymbol{M}\right]\left[\boldsymbol{G}\right]d\left\{\boldsymbol{u}\right\}_e\end{aligned} \tag{34}$$

In which, substituting $[\boldsymbol{M}]=[\boldsymbol{a}]^T[\overline{\boldsymbol{M}}][\boldsymbol{a}]$ into Eq. (12), we can obtained

$$\left[\boldsymbol{k}_\sigma\right]=\int_v[\boldsymbol{G}]^T[\boldsymbol{M}][\boldsymbol{G}]dv=\int_0^L[\boldsymbol{G}]^T[\hat{\boldsymbol{M}}][\boldsymbol{G}]dx \tag{35}$$

In which $[\hat{\boldsymbol{M}}]$ and $[\boldsymbol{G}]$ can be expressed as follows

$$[\hat{\boldsymbol{M}}]=\int_A[\boldsymbol{a}][\overline{\boldsymbol{M}}][a]dA$$

$$=\begin{bmatrix}
\sum_{i=1}^n\sigma_{11}A_i & 0 & 0 & 0 & \sum_{i=1}^n\sigma_{31}A_i & -\sum_{i=1}^n\sigma_{12}A_i & 0 & \sum_{i=1}^n\sigma_{11}z_iA_i & -\sum_{i=1}^n\sigma_{11}y_iA_i \\
0 & \sum_{i=1}^n\sigma_{11}A_i & 0 & -\sum_{i=1}^n\sigma_{31}A_i & 0 & 0 & -\sum_{i=1}^n\sigma_{11}z_iA_i & 0 & 0 \\
0 & 0 & \sum_{i=1}^n\sigma_{11}A_i & \sum_{i=1}^n\sigma_{12}A_i & 0 & 0 & \sum_{i=1}^n\sigma_{11}y_iA_i & 0 & 0 \\
0 & -\sum_{i=1}^n\sigma_{31}A_i & \sum_{i=1}^n\sigma_{12}A_i & 0 & 0 & 0 & \sum_{i=1}^n\left(\sigma_{31}z_i+\sigma_{12}y_i\right)A_i & 0 & 0 \\
\sum_{i=1}^n\sigma_{31}A_i & 0 & 0 & 0 & 0 & -\sum_{i=1}^n\sigma_{23}A_i & 0 & \sum_{i=1}^n\sigma_{31}z_iA_i & -\sum_{i=1}^n\sigma_{31}y_iA_i \\
-\sum_{i=1}^n\sigma_{12}A_i & 0 & 0 & 0 & -\sum_{i=1}^n\sigma_{23}A_i & 0 & 0 & -\sum_{i=1}^n\sigma_{12}z_iA_i & \sum_{i=1}^n\sigma_{12}y_iA_i \\
0 & -\sum_{i=1}^n\sigma_{11}z_iA_i & \sum_{i=1}^n\sigma_{11}y_iA_i & \sum_{i=1}^n\left(\sigma_{31}z_i+\sigma_{12}y_i\right)A_i & 0 & 0 & \sum_{i=1}^n\left(z_i^2+y_i^2\right)\sigma_{11}A_i & 0 & 0 \\
\sum_{i=1}^n\sigma_{11}z_iA_i & 0 & 0 & 0 & \sum_{i=1}^n\sigma_{31}z_iA_i & -\sum_{i=1}^n\sigma_{12}z_iA_i & 0 & \sum_{i=1}^n\sigma_{11}z_i^2A_i & -\sum_{i=1}^n\sigma_{11}z_iy_iA_i \\
-\sum_{i=1}^n\sigma_{11}y_iA_i & 0 & 0 & 0 & -\sum_{i=1}^n\sigma_{31}y_iA_i & \sum_{i=1}^n\sigma_{12}y_iA_i & 0 & -\sum_{i=1}^n\sigma_{11}z_iy_iA_i & \sum_{i=1}^n\sigma_{11}y_i^2A_i
\end{bmatrix}_{9\times9}$$

And

$$[\boldsymbol{G}]=\begin{bmatrix}
-\frac{1}{L} & 0 & 0 & 0 & 0 & 0 & \frac{1}{L} & 0 & 0 & 0 & 0 & 0 \\
0 & G_{2,2} & 0 & 0 & 0 & G_{2,6} & 0 & G_{2,8} & 0 & 0 & 0 & G_{2,12} \\
0 & 0 & G_{3,3} & 0 & G_{3,5} & 0 & 0 & 0 & G_{3,9} & 0 & G_{3,11} & 0 \\
0 & 0 & 0 & \frac{L-x}{L} & 0 & 0 & 0 & 0 & 0 & \frac{x}{L} & 0 & 0 \\
0 & 0 & G_{5,3} & 0 & G_{5,5} & 0 & 0 & 0 & G_{5,9} & 0 & G_{5,11} & 0 \\
0 & G_{6,2} & 0 & 0 & 0 & G_{6,6} & 0 & G_{6,8} & 0 & 0 & 0 & G_{6,12} \\
0 & 0 & 0 & -\frac{1}{L} & 0 & 0 & 0 & 0 & 0 & \frac{1}{L} & 0 & 0 \\
0 & 0 & G_{8,3} & 0 & G_{8,5} & 0 & 0 & 0 & G_{8,9} & 0 & G_{8,11} & 0 \\
0 & G_{9,2} & 0 & 0 & 0 & G_{9,6} & 0 & G_{9,8} & 0 & 0 & 0 & G_{9,12}
\end{bmatrix}$$

In which the components of $[\boldsymbol{G}]$ were expressed as following

$$G_{2,2}=\frac{(1-\Phi_z)L^2-6x(L-x)}{\Phi_z L^3},G_{2,6}=\frac{-2\Phi_z Lx-6x(L-x)+(1+\Phi_z)L^2}{2\Phi_z L^2},G_{2,8}=-G_{2,2},G_{2,12}=\frac{2\Phi_z Lx-6x(L-x)-(\Phi_z-1)L^2}{2\Phi_z L^2}$$

$$G_{3,3}=\frac{(1-\Phi_y)L^2+6x(x-L)}{\Phi_y L^3},G_{3,5}=\frac{2\Phi_y Lx-6x(x-L)-(1+\Phi_y)L^2}{2\Phi_y L^2},G_{3,9}=-G_{3,3},G_{3,11}=\frac{-2\Phi_y Lx-6x(x-L)-(1-\Phi_y)L^2}{2\Phi_y L^2}$$

$$G_{5,3}=\frac{6x(L-x)}{\Phi_y L^3},G_{5,5}=\frac{(3x-\Phi_y L)(x-L)}{\Phi_y L^2},G_{5,9}=-G_{5,3},G_{5,11}=\frac{(3x-3L+\Phi_y L)x}{\Phi_y L^2}$$

$$G_{6,2}=-\frac{6x(L-x)}{\Phi_z L^3},G_{6,6}=\frac{(3x-\Phi_z L)(x-L)}{\Phi_z L^2},G_{6,8}=-G_{6,2},G_{6,12}=\frac{(3x-3L+\Phi_z L)x}{\Phi_z L^2}$$

$$G_{8,3}=\frac{6(L-2x)}{\Phi_y L^3},G_{8,5}=\frac{6x-3L-\Phi_y L}{\Phi_y L^2},G_{8,9}=-G_{8,3},G_{8,11}=\frac{6x-3L+\Phi_y L}{\Phi_y L^2}$$

$$G_{9,2}=-\frac{6(L-2x)}{\Phi_z L^3},G_{9,6}=\frac{6x-3L-\Phi_z L}{\Phi_z L^2},G_{9,8}=-G_{9,2},G_{9,12}=\frac{6x-3L+\Phi_z L}{\Phi_z L^2}$$

3.3 Derivation large displacement stiffness matrix

Large displacement stiffness matrix ${}^t[\boldsymbol{k}_U]^e$ was induced by only considering the effect of three translational displacements of nodal point

$$\boldsymbol{\varepsilon}_{NL}=\left\{\frac{du}{dx}\quad\frac{dv}{dx}\quad\frac{dw}{dx}\quad 0\quad 0\quad 0\right\}\begin{bmatrix}\frac{1}{2}&0&0&0&0&0\\0&\frac{1}{2}&0&0&0&0\\0&0&\frac{1}{2}&0&0&0\\0&0&0&0&0&0\\0&0&0&0&0&0\\0&0&0&0&0&0\end{bmatrix}\begin{Bmatrix}\frac{du}{dx}\\\frac{dv}{dx}\\\frac{dw}{dx}\\0\\0\\0\end{Bmatrix}\tag{36}$$

Where, $\frac{\partial u}{\partial x},\frac{\partial v}{\partial x}$ and $\frac{\partial w}{\partial x}$ were expressed as follows

$$\begin{Bmatrix}\frac{du}{dx}\\\frac{dv}{dx}\\\frac{dw}{dx}\\0\\0\\0\end{Bmatrix}=\begin{Bmatrix}\frac{du}{dx}\\\frac{dv}{dx}\\\frac{dw}{dx}\\0\\0\\0\end{Bmatrix}=[\tilde{\boldsymbol{G}}]\{\boldsymbol{u}\}_e\tag{37}$$

Nonlinear Incremental strain $\boldsymbol{\varepsilon}_{NL}$ can be expressed as the matrix form

$$\begin{aligned}\boldsymbol{\varepsilon}_{NL} &= \frac{1}{2}\left(\{\boldsymbol{u}\}^e\right)^T[\tilde{\boldsymbol{G}}]^T[\boldsymbol{a}][\tilde{\boldsymbol{G}}]\{\boldsymbol{u}\}^e \\ &= \frac{1}{2}[\boldsymbol{A}][\tilde{\boldsymbol{G}}]\{\boldsymbol{u}\}^e\end{aligned} \tag{38}$$

Where, $[\boldsymbol{A}] = (\{\boldsymbol{u}\}_e)^T[\tilde{\boldsymbol{G}}][\boldsymbol{a}]$,

In which $[\boldsymbol{a}]$ can be defined as the following matrix,

$$[\boldsymbol{a}] = \begin{bmatrix} 1 & 0 & 0 & 0 & 0 & 0 \\ 0 & 1 & 0 & 0 & 0 & 0 \\ 0 & 0 & 1 & 0 & 0 & 0 \\ 0 & 0 & 0 & 0 & 0 & 0 \\ 0 & 0 & 0 & 0 & 0 & 0 \\ 0 & 0 & 0 & 0 & 0 & 0 \end{bmatrix}$$

$\boldsymbol{\varepsilon}_{NL}$ was derived by calculus of variation, we obtain

$$\delta\boldsymbol{\varepsilon}_{NL} = \delta\left(\frac{1}{2}[\boldsymbol{A}][\tilde{\boldsymbol{G}}]\{\boldsymbol{u}\}^e\right) = \boldsymbol{B}_{NL}\{\delta\boldsymbol{u}\}^e \tag{39}$$

Where

$$\boldsymbol{B}_{NL} = [\boldsymbol{A}][\tilde{\boldsymbol{G}}] \tag{40}$$

$[\tilde{\boldsymbol{G}}]$ can be particularly expressed in matrix form,

$$[\tilde{\boldsymbol{G}}] = \begin{bmatrix} -\frac{1}{L} & 0 & 0 & 0 & 0 & 0 & \frac{1}{L} & 0 & 0 & 0 & 0 & 0 \\ 0 & -\frac{6x}{L^2}+\frac{6x^2}{L^3} & 0 & 0 & 0 & 1-\frac{4x}{L}+\frac{3x^2}{L^2} & 0 & \frac{6x}{L^2}-\frac{6x^2}{L^3} & 0 & 0 & 0 & -\frac{2x}{L}+\frac{3x^2}{L^2} \\ 0 & 0 & -\frac{6x}{L^2}+\frac{6x^2}{L^3} & 0 & \frac{4x}{L}-\frac{3x^2}{L^2}-1 & 0 & 0 & 0 & \frac{6x}{L^2}-\frac{6x^2}{L^3} & 0 & \frac{2x}{L}-\frac{3x^2}{L^2} & 0 \\ 0 & 0 & 0 & 0 & 0 & 0 & 0 & 0 & 0 & 0 & 0 & 0 \\ 0 & 0 & 0 & 0 & 0 & 0 & 0 & 0 & 0 & 0 & 0 & 0 \\ 0 & 0 & 0 & 0 & 0 & 0 & 0 & 0 & 0 & 0 & 0 & 0 \end{bmatrix}$$

We obtained the linear strain stiffness matrix in local coordinate system

$${}^t[\boldsymbol{k}_L]^e = \int_L [\boldsymbol{B}_L]^T[\boldsymbol{k}_s][\boldsymbol{B}_L]dx \tag{41}$$

We obtained the large displacement stiffness matrix in the ordinate system

$${}^t[\boldsymbol{k}_U]^e = \frac{1}{2}\left(\int_L [\boldsymbol{B}_L]^T[\boldsymbol{k}_s][\boldsymbol{B}_{NL}]dx + \int_L [\boldsymbol{B}_{NL}]^T[\boldsymbol{k}_s][\boldsymbol{B}_L]dx + \int_L [\boldsymbol{B}_{NL}]^T[\boldsymbol{k}_s][\boldsymbol{B}_{NL}]dx\right) \tag{42}$$

We obtained the geometric stiffness matrix in the local ordinate system

$${}^t[\boldsymbol{k}_\sigma]^e = \int_v [\boldsymbol{G}]^T[\boldsymbol{M}][\boldsymbol{G}]dv = \int_0^L [\boldsymbol{G}]^T[\hat{\boldsymbol{M}}][\boldsymbol{G}]dx \tag{43}$$

Eqs. (41), (42), (43) were transformed to the global coordinate system by multiplying the transformation matrix, at last we obtained nonlinear incremental U.L. formulation equilibrium equation in the global coordinate system as following

$$\left([{}^{t+\Delta t}_{\ \ t}\boldsymbol{K}_L]+[{}^{t+\Delta t}_{\ \ t}\boldsymbol{K}_\sigma]+[{}^{t+\Delta t}_{\ \ t}\boldsymbol{K}_U]\right)\{\Delta\boldsymbol{U}\}=\{\boldsymbol{F}_{t+\Delta t}\}-\{\boldsymbol{f}_t\} \tag{44}$$

Where, $[{}^{t+\Delta t}_{\ \ t}\boldsymbol{K}_L]$ was linear strain stiffness matrix in the global coordinate system, $[{}^{t+\Delta t}_{\ \ t}\boldsymbol{K}_\sigma]$ was geometric stiffness matrix in the global coordinate system, $[{}^{t+\Delta t}_{\ \ t}\boldsymbol{K}_U]$ was the large displacement stiffness matrix in the global coordinate system, $\{\boldsymbol{F}_{t+\Delta t}\}$ was external $f_{t+\Delta t}$ force vector in the global coordinate system, $\{\boldsymbol{f}_t\}$ was resisting force vector of element.

The incremental nonlinear equilibrium equation was solved by modified arc-length method (Riks 1979, Crisfield 1983).

5 Finite rotation by updating of element geometry

Since the law of commutativity remains valid for small rotations about the three axes, the end rotational angles of each element can be calculated simply by adding the rotational angles increments generated at the current load step to those accumulated up to the previous load step. Thus with the assumption of small rotations, the procedure for updating the end orientations becomes a trivial task. However, for the cases where finite rotation happens, the above procedure for updating the end orientations of each element in the three dimensional space had to be developed based on the theory of finite rotation in order to account for the effect of noncommutativity. Furthermore the vector finitely rotates about one axes, the rotational angle can not be linearly added to those accumulated up to the previous load step (Oran 1973).

Finite rotation by updating of element geometry was based on the research of Yang (1994). The main idea of his research was based on the assumption of rigid joints between the centroid of cross-section and nodal point of element, the three translational displacements can be linearly add to the previous load step, but the rotational displacements can only be calculated by Euler's finite rotation formula. The coordinate vectors of centroid of cross-section was obtained by transformation matrix, and the coordinate vectors of two nodal sections were mapped to the normal section of middle point of the connecting line of two deformed end nodal points. The major and minor principal directions were obtained of two end nodal points, and then were normalized including some geometric settlement in order to deduct the rigid displacements (Argyris *et al.* 1982), concrete procedure was derived as following.

5.1 Updating of Nodal point coordinate of element

Nodal translational displacement increment $\Delta\boldsymbol{u}$ and rotational displacement increment $\Delta\boldsymbol{\theta}$ can be expressed as following for the time t configuration to the time $t+\Delta t$ configuration

$$\Delta\boldsymbol{u}=\Delta u_x i+\Delta u_y j+\Delta u_z k \tag{45}$$

$$\Delta\boldsymbol{\theta}=\Delta\theta_x i+\Delta\theta_y j+\Delta\theta_z k \tag{46}$$

The magnitude ϕ and unit direction vector $\vec{n}$ of the rotation increment $\Delta\boldsymbol{\theta}$ were as follows

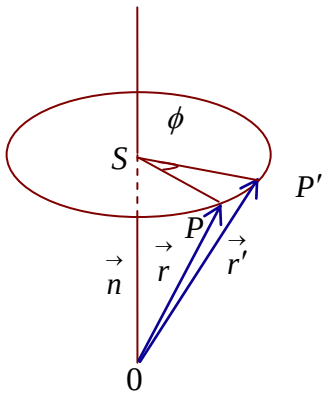

Fig. 2 Finite rotation for element node

$$\vec{\boldsymbol{n}} = \frac{\Delta\boldsymbol{\theta}}{\phi} \tag{47}$$

Where, $\phi = \sqrt{\Delta\theta_x^2 + \Delta\theta_y^2 + \Delta\theta_z^2}$, according to Euler's finite rotation formula, see Fig. 2, ${}^{t+\bar{\Delta}t}\xi$, ${}^{t+\bar{\Delta}t}\eta$, ${}^{t+\bar{\Delta}t}\zeta$ of nodal coordinate in the t+Δt configuration were obtained in the following

$$\begin{aligned}
{}^{t+\Delta t}\vec{\boldsymbol{\xi}} &= \cos\phi\, {}^{t}\vec{\boldsymbol{\xi}} + \sin\phi\left(\vec{\boldsymbol{n}} \times {}^{t}\vec{\boldsymbol{\xi}}\right) + (1-\cos\phi)\left(\vec{\boldsymbol{n}} \cdot {}^{t}\vec{\boldsymbol{\xi}}\right)\vec{\boldsymbol{n}} \\
{}^{t+\Delta t}\vec{\boldsymbol{\eta}} &= \cos\phi\, {}^{t}\vec{\boldsymbol{\eta}} + \sin\phi\left(\vec{\boldsymbol{n}} \times {}^{t}\vec{\boldsymbol{\eta}}\right) + (1-\cos\phi)\left(\vec{\boldsymbol{n}} \cdot {}^{t}\vec{\boldsymbol{\eta}}\right)\vec{\boldsymbol{n}} \\
{}^{t+\Delta t}\vec{\boldsymbol{\zeta}} &= \cos\phi\, {}^{t}\vec{\boldsymbol{\zeta}} + \sin\phi\left(\vec{\boldsymbol{n}} \times {}^{t}\vec{\boldsymbol{\zeta}}\right) + (1-\cos\phi)\left(\vec{\boldsymbol{n}} \cdot {}^{t}\vec{\boldsymbol{\zeta}}\right)\vec{\boldsymbol{n}}
\end{aligned} \tag{48}$$

5.2 Calculation of element natural deformation

For the purpose of calculating the element inner forces at each incremental iteration step, the displacement increments $\{\boldsymbol{u}\}$ solved from the nonlinear incremental equilibrium equation can be decomposed (Belytschko and Hsieh 1973, Nour-Omid and Rankin 1991, Crisfield and Moita 1996, Li *et al.* 2011, Cai and Atluri 2012, Pramin and Ki 2012) into two parts: the rigid body displacements $\{\boldsymbol{u}\}_r$ and the natural deformations $\{\boldsymbol{u}\}_n$

$$\{\boldsymbol{u}\} = \{\boldsymbol{u}\}_r + \{\boldsymbol{u}\}_n \tag{49}$$

Through the rigid displacement, ${}^{t}x$, ${}^{t}y$, ${}^{t}z$ in the time t configuration was transformed to ${}^{t+\Delta t}x$, ${}^{t+\Delta t}y$, ${}^{t+\Delta t}z$ in the time t+Δt configuration, see Fig. 3, natural deformation $\{\boldsymbol{u}\}_n$ was expressed as following referring to the time t+Δt configuration

$$\{\boldsymbol{u}\}_n = \{0 \quad 0 \quad 0 \quad \theta_{xi} \quad \theta_{yi} \quad \theta_{zi} \quad \Delta u \quad 0 \quad 0 \quad \theta_{xj} \quad \theta_{yj} \quad \theta_{zj}\}^T \tag{50}$$

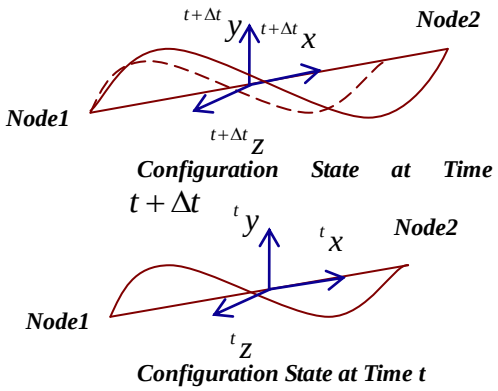

Fig. 3 Rigid body displacements and natural deformations

Where Δu can be written as follows

$$\Delta u = {}^{t+\Delta t}L - {}^{t}L \tag{51}$$

Where, ${}^{t+\Delta t}L$ was the length of element in the $t+\Delta t$ configuration, ${}^{t}L$ was the length of element in the t configuration, the node i of element rotational displacements were expressed as follows

$$\{\theta_{xi} \quad \theta_{yi} \quad \theta_{zi}\} = \phi\{\boldsymbol{n}_i\}^T \tag{52}$$

In which ϕ, $\{n_i\}$

$$\phi = \sin^{-1}\left(\frac{\lambda}{2}\right) \tag{53}$$

$$\lambda = \sqrt{(\gamma_2 - \beta_3)^2 + (\alpha_3 - \gamma_1)^2 + (\beta_1 - \alpha_2)^2} \tag{54}$$

$$\{\boldsymbol{n}_i\} = \left[\{{}^{t}_{0}\alpha\} \quad \{{}^{t}_{0}\beta\} \quad \{{}^{t}_{0}\gamma\}\right]\{{}_{t}n_i\} \tag{55}$$

$$\{{}_{t}\boldsymbol{n}_i\} = \left\{-\frac{\gamma_2 - \beta_3}{\lambda} \quad -\frac{\alpha_3 - \gamma_1}{\lambda} \quad -\frac{\beta_1 - \alpha_2}{\lambda}\right\}^T \tag{56}$$

$$\{{}^{k}_{0}\boldsymbol{p}_i\} = [{}^{k}\boldsymbol{R}]^T\{{}^{k}\boldsymbol{q}_i\}(k = t, t+\Delta t; p = \alpha, \beta, \gamma; q = \xi, \eta, \zeta) \tag{57}$$

$$[{}^{k}\boldsymbol{R}] = [\{{}^{k}x\} \quad \{{}^{k}y\} \quad \{{}^{k}z\}](k = t, t+\Delta t) \tag{58}$$

$$\{{}^{t+\Delta t}_{t}\boldsymbol{p}_i\} = \left[\{{}^{t}_{0}\alpha_i\} \quad \{{}^{t}_{0}\beta_i\} \quad \{{}^{t}_{0}\gamma_i\}\right]^T\{{}^{t+\Delta t}_{0}\boldsymbol{p}_i\}(p = \alpha, \beta, \gamma) \tag{59}$$

$$\begin{aligned} \{{}^{t+\Delta t}_{t}\boldsymbol{\alpha}_i\} &= \{\alpha_1 \quad \alpha_2 \quad \alpha_3\}^T \\ \{{}^{t+\Delta t}_{t}\boldsymbol{\beta}_i\} &= \{\beta_1 \quad \beta_2 \quad \beta_3\}^T \\ \{{}^{t+\Delta t}_{t}\boldsymbol{\gamma}_i\} &= \{\gamma_1 \quad \gamma_2 \quad \gamma_3\}^T \end{aligned} \tag{60}$$

Eqs. (53)-(60), $\{\boldsymbol{\alpha}_i\}$, $\{\boldsymbol{\beta}_i\}$, $\{\boldsymbol{\gamma}_i\}$ was the vector of cross-section centroid coordinate system ($\alpha_i \beta_i \gamma_i$), Substituting (53)-(60) into Eq. (52), the rotational vector of i nodal point (Node 1) of element. Similar procedures can be followed to calculate the natural rotations of the element at node j (Node 2).

6 Numerical examples and discussion

6.1 Cantilever beam under concentrated moment finite rotation analysis

The example of a cantilever beam subjected to a concentrated moment at the free end was illustrated in Fig. 4. This classical problem had been analyzed by many outstanding researchers, including Bathe and Bolourch (1979), Schulz and Filippou (2001). It is very clearly that the exact solution for the deformed shape of this structure is a perfect circle, since the bending moment is constant along the cantilever beam. The length of the beam L was 8 m, and it was discretized into eight beam elements, with cross-section 1 m×1 m.The modulus of elasticity was 210 GPa, the passion ratio was zero, and shear modulus was 105 GPa. The concentrate bending moment $M=k\pi EI/L$ was applied to the free end, with k=0.1, k=0.9, k=0.8, k=0.7, k=0.6, k=0.5, k=0.4, k=0.3, k=0.2, k=0.1 be analyzed respectively. The curves shown Fig. 5 was in fantastic agreement with the analytical solution.

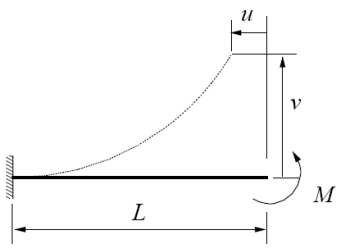

Fig. 4 Cantilever beam subjected to concentrate moment

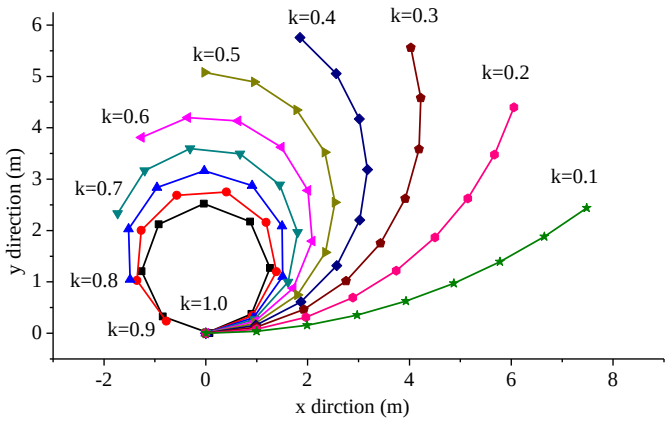

Fig. 5 Configuration of the deformed cantilever beam corresponding to different k

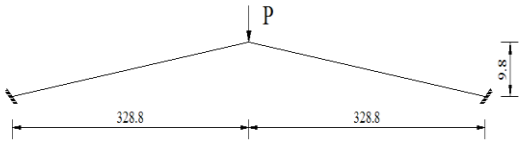

Fig. 6 Geometry of William's toggle frame (Unit: mm)

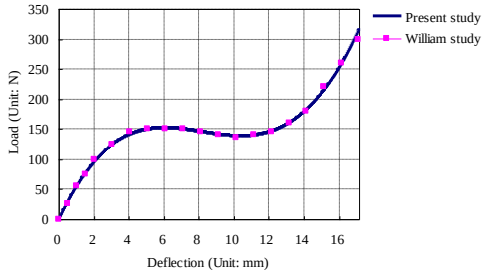

Fig. 7 Load-deflection curves for William's toggle frame

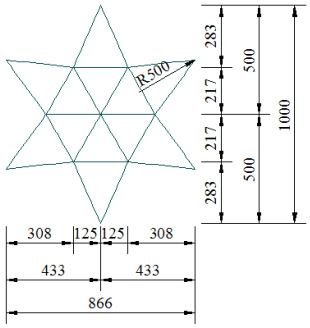

Fig. 8 Plane figure for hexagonal star-shaped shallow dome (Unit: mm)

6.2 Williams's toggle frame analysis

This example, see Fig. 6, had been solved analytically and experimentally tested by Williams (1964). It was a toggle frame with two fixed ends, its cross-section was rectangular 19.13 mm×6.17 mm, and modulus of elasticity was 71018.5 MPa. When Williams analyzed the structure, the effects of finite deflections and rotations including flexural shorting of member were taken into consideration, including the axial forces on the flexural stiffness. When the structure was calculated, every element was devised into six elements, the cross-section was devised into three fibers and two fibers along height and along width respectively. The analysis results were in strong close agreement with the analytical solved by Williams, please see Fig. 7.

6.3 24-Member shallow dome analysis

The structure shown Fig. 8 and Fig. 9 had been analyzed by many well-known authors

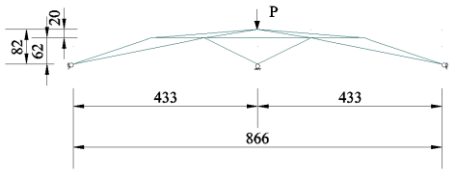

Fig. 9 Vertical figure for hexagonal star-shaped shallow dome (Unit: mm)

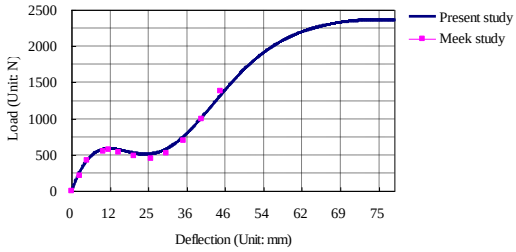

Fig. 10 Load-deflection curves for hexagonal star-shaped shallow dome

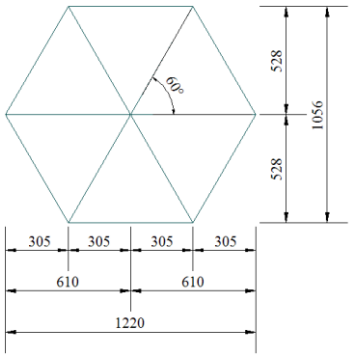

Fig. 11 Plane figure for hexagonal frame (Unit: mm)

(Papadrakakis 1981, Watson and Holzer 1983, Meek and Tan 1984)as a spatial frame or spatial truss to trace its load-deflection behavior into the post-buckling range. The boundary condition of the structure was hinged, and its cross-section property: I_y=23771 mm^4, I_z=9181 mm^4, A=317 mm^2. The property of material: modulus of elasticity was 3030 MPa,shear modulus was 1096 MPa. The results presented its post-buckling load-deflection path were in very close agreement with the analytical solved by Meek (1984), please see Fig. 10.

6.4 12-Member hexagonal frame analysis

The hexagonal frame shown Fig. 11 and Fig. 12 had been experimentally by studied by Griggs (1996), the pre-buckling and post-buckling range behavior had been calculated by Papadrakakis (1981), whose results was in exact agreement with that of experimental result, considering the effects of large displacement and finite rotation. The boundary condition of the structure was hinged, its cross-area was square 17.9 mm×17.9 mm. The modulus of elasticity was 3030 MPa, and shear modulus was 1096 MPa, when the structure was calculated by author, every member

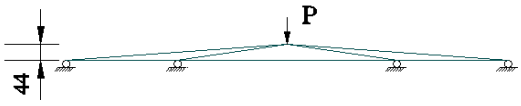

Fig. 12 Vertical plane figure for hexagonal frame (Unit:mm)

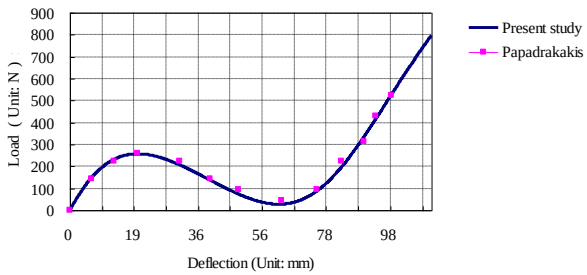

Fig. 13 Load-deflection curves for hexagonal frame

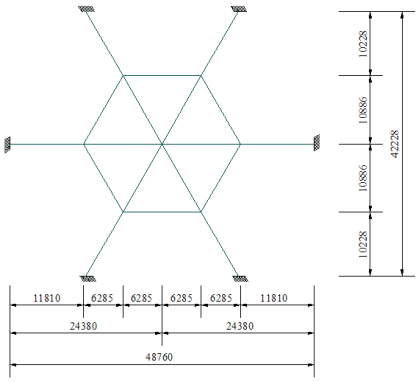

Fig. 14 Plane figure for Remseth's framed dome (Unit: mm)

was simulated by three elements, the cross-section was segmented into four fibers along height and along width respectively, and every member was discretized into four elements. The curve of Fig. 15 is excellent agreement with Papadrakakis' analysis results. Fig. 13 also indicates that the fiber beam element can accurately simulate highly nonlinear relationship of load-deflection of the pre-buckling and post-buckling of spatial structure under ultimate load, considering large displacement and finite rotation.

6.5 Remseth spatial framed dome analysis

Remseth spatial framed dome shown Fig. 14 and Fig. 15 was chosen. The structure was once analyzed by Chu and Rampetsreiter (1972), Shi and Atluri (1988), Park and Lee (1996). The six boundary nodal points were fixed in all the direction, cross-section was rectangular 0.76 m×1.22 m. The modulus elasticity was 20690 MPa, shear modulus was 8621 MPa. Each of member was simulated by a single fiber beam element, cross-section were subdivided into 8 by 14 fibers. Based on the complementary energy approach, Shi analyzed the structure by using an element to simulate

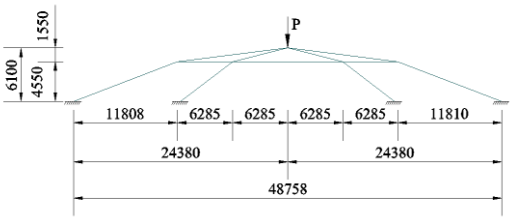

Fig. 15 Vertical plane figure for Remseth's framed dome (Unit: mm)

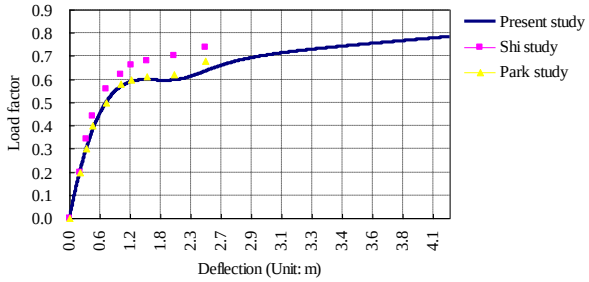

Fig. 16 Load-deflection curves for Remseth's framed dome

Table 1 Material properties of concrete

Material parameter	f_c/MPa	ε_0	f_{cu}/MPa	ε_u
Confined concrete area	-32.05	-0.0022	-29.20	-0.014
Unconfined concrete area	-29.20	-0.0020	0	-0.006

a member considering large displacement, finite rotation, and the nonlinear bending-stretching coupling; while Park analyzed the structure by utilizing 16 elements to model a member, and cross-section was discretized 14 by 8 Gauss points along wide and narrow principal directions respectively considering elastoplastic material and geometric nonlinear, and then the analysis result of pre-bulcking and large deflection collapse of spatial framed structures were presented. The present analysis result curve shown Fig. 16 was in favorable agreement with Shi's result and Park's result.

6.6 push-over analysis of reinforced concrete pier column

See Fig. 17 the pier column was numerically simulated by utilizing one fiber beam element, and cross-area was discretized twenty-four unconfined concrete fibers, eighteen steel bars, and then the confined concrete area in the core was discretized thirty-two confined concrete fibers, forty confined concrete fibers, sixty-four confined concrete fibers respectively. Constitutive model of unconfined concrete and confined concrete (Taucer *et al.* 1991) was used. Material parameters, such as peak compressive stress f_c, peak compressive strain ε_0, limit compressive stress f_{cu}, limit compressive strain ε_{cu}, please see Table 1. Constitutive model of steel bar [42] was used in this example. Material parameters, such as initial elastic modulus E_{s0}=200 GPa, yield strength f_y=357 Mpa, stiffness hardening coefficient after yield b=0.01.

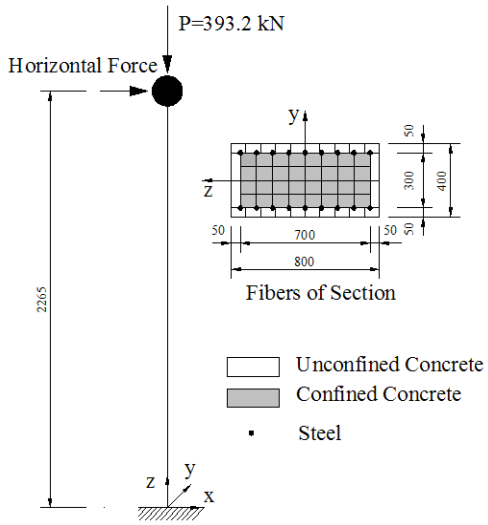

Fig. 17 Element and section discretization for RC pier (Unit: mm)

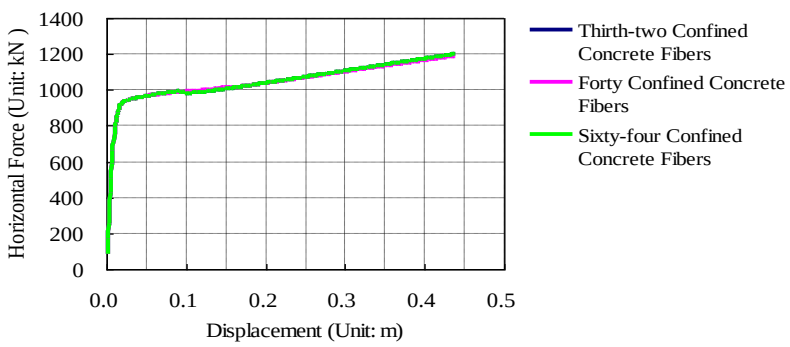

Fig. 18 Horizontal force - horizontal displacement curves for RC pier

In Fig. 18, the numerical results tend to be uniform with the confined concrete area discretized thirty-two fibers, forty fibers, and sixty-four fibers respectively. When the displacement of pier top reached 0.438 m, the bearing capacity of the pier was close to be the limit state, and the failure occurred. Especially, when the displacement of the pier top was close to be 0.012 m~0.438 m, strongly nonlinear characteristics occurred. So, the large displacement and finite rotation should be considered in the analytical process.

7. Conclusions

Firstly, based on continuum mechanics and the principle of virtual displacements, incremental T.L. formulation and incremental U.L. formulation were presented, in which the large displacement matrix was taken into consideration, and then was modified to be symmetrical matrix. Secondly, three dimensional Timoshenko fiber beam element was formulated base on U.L.

in the assumption small strain, large displacement, finite rotation. Finally, through several examples, some valuable and practical conclusion can be obtained as follows:

• The three dimensional Timoshenko fiber beam was an accurate beam element to simulate the spatial framed structure; large displacement, finite rotation analysis can be solved through relatively large load step and large displacement increments.

• The fiber beam can highly accurately simulate the highly nonlinear pre-buckling and post-buckling analysis, and structure progressive collapse analysis can be really numerically simulated by utilizing this fiber beam element.

• It can be shown that the fiber beam element can be used efficiently for large displacement geometrically nonlinear analysis of spatial framed structures.

Acknowledgments

The research described in this paper was financially supported by the Natural Science Foundation of China (Project No. 51178331).

References

Argyris, J.H., Boni, B., Hindenlang, U. and Kleiber, M. (1982), "Finite element analysis of two- and three-dimensional elasto-plastic frames- the natural approach", *Comput. Meth. Appl. Mech. Eng.*, **35**(2), 221-248.

Bathe, K.J. (1982), *Finite Element Procedures in Engineering Analysis*, Prentice-Hall, New Jersey, USA.

Bathe, K.J. and Bolourch, I.S. (1979), "Large displacement analysis of three-dimensional beam structures", *Int. J. Numer. Meth. Eng.*, **14**(7), 961-986.

Bathe, K.J., Ramm. E. and Wilson. E.L. (1975), "Finite element formulations for large deformation dynamic analysis", *Int. J. Numer. Meth. Eng.*, **9**(2), 353-386.

Bathe, K.J. and Wilson, E.L. (1974), "Nonsap-a nonlinear structural analysis program", *Nucl. Eng. Des.*, **29**(2), 266-293.

Bazoune, A., Khulief, Y.A. and Stephen, N.G. (2003), "Shape functions of three-dimensional Timoshenko beam element", *J. Sound. Vib.*, **259**(2), 473-480.

Belytschko, T. and Hsieh, B.J. (1973), "Non-linear transient finite element analysis with convected co-ordinates", *Int. J. Numer. Meth. Eng.*, **7**(3), 255-271.

Cai, Y.C. and Atluri, S.N. (2012), "Large rotation analyses of plate/shell structures based on the primal variational principle and a fully nonlinear theory in the updated Lagrangian co-rotational reference frame", *CMES-Comp. Model. Eng.*, **83**(3), 49-273.

Chu, K.H. and Rampetsreiter, R.H. (1972), "Large deflection buckling of space frames", *J. Struct. Div.*, **98**(12), 2701-2722.

Crisfield, M.A. (1983), "An arc-length method including line searches and accelerations", *Int. J. Numer. Meth. Eng.*, **19**(9), 1269-1289.

Crisfield, M.A. and Moita. G.F. (1996), "A unified co-rotational frame work for solids, shells and beams", *Int. J. Solid. Struct.*, **33**(20-22), 2969-2992.

Crivelli, L.A. and Felippa, C.A. (1993), "A three dimensional nonlinear Timoshenko beam based on the core-congruential formulation", Int*. J. Numer. Meth. Eng.*, **36**(21), 3647-3673.

Eduardo, N.D., Eugenio, O. and Javier, O. (1988), "On a non-linear formulation for curved Timoshenko beam elements considering large displacement/rotation increments", *Int. J. Numer. Meth. Eng.*, **26**(7), 1597-1613.

Griggs, H.P. (1996), "Experimental study of instability in elements of shallow space frames", Research

Reprot, Dept. of Civil Eng, MIT, Cambridge, USA.
Hibbitt, H.D., Marcal, P.V. and Rice, J.R. (1970), "A finite element formulation for problems of large strain and large displacement", *Int. J. Solid. Struct*., **6**(8), 1069-1086.
Huu, T.T. and Seung, E.K. (2011a), "Second-order inelastic dynamic analysis of steel frames using fiber hinge method", *J. Constr. Steel Res*., **67**(10), 1485-1494.
Huu, T.T. and Seung, E.K. (2011b), "Nonlinear inelastic analysis of concrete-filled steel tubular frames", *J. Constr. Steel Res.*, **67**(12), 1797-1805.
Huu, T.T. and Seung, E.K. (2012), "Second-order inelastic analysis of cable-stayed bridges", *Finite Elem. Anal. Des.*, **53**, 48-55.
Li, Y., Lu, X.Z., Ye, L.P. and Ren, A.Z. (2012), "Numerical models of fire induced progressive collapse analysis for reinforced concrete frame structures", *Eng. Mech*., **29**(4), 96-103.
Li, Z.X., Liu, Y.F., Izzuddin, B.A. and Vu-Quoc, L.A. (2011), "Stabilized co-rotational curved quadrilateral composite shell element", *Int. J. Numer. Meth. Eng*., **86**(8), 975-999.
Li, Z.X. and Izzuddin, B.A. (2011), "A mixed co-rotational curved quadrilateral shell element", *Int. J. Struct. Eng*., **2**(2), 188-208.
Meek, J.L. and Tan, H.S. (1984), "Geometrically nonlinear analysis of space frames by an incremental iterative technique", *Comput. Meth. Appl. Mech. Eng*., **47**(3), 261-282.
Nie, J.G. and Wang, Y.H. (2012), "Development and application of steel-concrete composite fiber beam model in ABAQUS platform", *Eng. Mech*., **29**(1), 70-80.
Nour-Omid, B. and Rankin, C.C. (1991), "Finite rotation analysis and consistent linearization using projectors", *Comput. Meth. Appl. Mech. Eng*., **93**(3), 353-384.
Oran, C. (1973), "Tangent stiffness in space frames", *J. Struct. Div*., **99**(6), 987-1001.
Papadrakakis, M. (1981), "Post-buckling analysis of spatial structures by vector iteration methods", *Comput. Struct*., **14**(5-6), 393-402.
Park, M.S. and Lee, B.C. (1998), "Geometrically non-linear and elastoplastic three dimensional shear flexible beam element of von-mises-type hardending material", *Int. J. Numer. Meth. Eng*., **39**(3), 383-408.
Pramin, N., Songsak, S. and Ki, K. (2012), "A co-rotational 8-node degenerated thin-walled element with assumed natural strain and enhanced assumed strain", *Finite Elem. Anal. Des*., **50**, 70-85.
Riks, E. (1979), "An incremental approach to the solution of snapping and buckling problems", *Int. J. Solid. Struct*., **15**(7), 529-551.
Schulz, M. and Filippou, F.C. (2001), "Non-linear spatial Timoshenko beam element with curvature interpolation", *Int. J. Numer. Meth. Eng*., **50**(4), 761-785.
Shi, G. and Atluri, S.N. (1988), "Elasto-plastic large deformation analysis of space-frames: a plastic-hinge and stress-based explicit derivation of tangent stiffnesses", *Int. J. Numer. Meth. Eng*., **26**(3), 589-615.
Spacone, E., Filippou, F.C. and Taucer, F.F. (1996a), "Fiber beam-column model for nonlinear analysis of R/C frames: part I. Formulation", *Earthq. Eng. Struct*., **25**(7), 711-725.
Spacone, E., Filippou, F.C. and Taucer, F.F. (1996b), "Fiber beam-column model for nonlinear analysis of R/C frames: part II. Applications", *Earthq. Eng Struct*, **25**(7), 727-742.
Taucer, F.F., Spacone, E. and Filippou, F.C. (1991), "A Fiber Beam-Column Element for Seismic Response Analysis of Reinforced Concrete Structures", EERC Report 91/17, Earthquake Engineering Research Center, University of California.
Tort, C. and Hajjar, J. (2010), "Mixed finite element for three-dimensional nonlinear dynamic analysis of rectangular concrete-filled steel tube beam-columns", *J. Eng. Mech*., **136**(11), 1329-1339.
Yang, Y.B. (1994), *Theory and Analysis of Nonlinear Framed Structures*, Prentice-Hall, New Jersey, USA.
Watson, L.T. and Holzer, S.M. (1984), "Quadratic convergence of crisfield's method", *Comput. Struct*., **17**(1), 69-72.
William, F.W. (1964), "An approach to the non-linear behaviour of the members of a rigid jointed plane framework with finite deflections", *Q. J. Mech. Appl. Math*., **17**(4), 451-469.
Zeris, C.A. and Mahin, S.A. (1988), "Analysis of reinforced concrete beam-columns under uniaxial excitation", *J. Struct. Eng*., **114**(4), 804-820.
Zeris, C.A. and Mahin, S.A. (1991), "Behavior of reinforced concrete structures subjected to biaxial

excitation", *J. Struct. Eng*., **117**(9), 2657-2673.

Zhang, L.X., Xu, G.L. and Bai, Y.S. (2011), "Fiber model based on Timoshenko beam theory and its application", *Adv. Sci. Lett*., **4**(4-5), 1886-1888.

Zubydan, A.H. and ElSabbagh, A.I. (2011), "Monotonic and cyclic behavior of concrete-filled steel-tube beam-columns considering local buckling effect", *Thin Wall. Struct*., **49**(4), 465-481.